Adiabatic refocusing of nuclear spins in Tm³⁺:YAG

R. Lauro, T. Chanelière, and J.-L. Le Gouët[*]

Laboratoire Aimé Cotton, CNRS UPR3321, Univ. Paris Sud, Bâtiment 505, Campus Universitaire, 91405 Orsay, France

We show that the optical absorbance detection of nuclear spin echo gives direct access to the spin concentration, unlike most coherent signal detection techniques where the signal intensity/amplitude is difficult to connect experimentally with the spin concentration. This way we measure the spin-refocusing efficiency in a crystal of Tm³⁺:YAG. Given the large inhomogeneous broadening of the spin transition in this material, rephasing the spins with the usual hard pulse procedure would require excessively high radiofrequency power. Instead we resort to an adiabatic pulse sequence that perfectly returns the spins to their initial common orientation, at low power cost.

I. INTRODUCTION

The optical detection of magnetic resonance has been investigated for a long time, starting with atomic vapors.[1–3] In solids, the earliest studies were reported in ruby.[4] Since the emergence of tunable lasers, special attention has been paid to the Raman heterodyne optical detection of coherent transient spin processes.[5] Detection of coherent magnetic resonance features through optical fluorescence was examined even earlier.[6] In the latter class of processes, a $\pi/2$ rf pulse is used to convert the spin coherence into a level population that can emit light by fluorescence. A similar approach was also used to detect spin echoes through optical absorbance.[7]

Optically detected magnetic resonance is enjoying renewed interest as research on quantum memory for light becomes more popular. Most quantum storage schemes rely on the conversion of optical atomic coherence into long-lifetime spin coherence and back.[8–12] Echo techniques are needed to compensate for the spin-inhomogeneous phase shift,[13,14] that is, to refocus the spins.

In the present paper our aim is twofold. First, we examine the potential of adiabatic rapid passage (ARP) for spin refocusing, when hard pulses would require excessive rf power. Second, placing this research in the context of quantum memory, we explore the specificity of magnetic resonance detection through the absorption of light. We show that this approach may convey more information than the direct detection of coherent emission. This relies on the fact that an absorption coefficient is related to the concentration of absorbing centers in a simple and precise way.

After discussing the principle of adiabatic spin refocusing in Sec. II, we present the absorbance detection of spin refocusing in Secs. III and IV. The experiment, described in Sec. V, is conducted in Tm³⁺:YAG, an actively investigated system in the prospect of quantum storage.[11,15–20]

II. ADIABATIC SPIN REFOCUSING

When spins interact with a spatially nonuniform static vertical magnetic field, the energy level spacing is inhomogeneously broadened. Then, excitation by a rf horizontal pulse gives rise to an oscillating magnetization that rapidly vanishes as the various spins precess at different rates around the static field. It is well known that a π pulse can rephase the spins and restore the oscillating horizontal magnetization. In order to uniformly excite all the spins, this pulse must be shorter than the inverse inhomogeneous broadening. This condition may entail inaccessible or unrealistic rf power requirements. Indeed, at a given pulse area, the needed rf power varies as the square of the inverse pulse duration. By successively driving the spins with different energy level spacings, frequency-chirped rf pulses may offer a less power-demanding way of excitation. This is precisely the way ARP works.

Since the early days of nuclear magnetic resonance (NMR), ARP has been extensively used to flip vertically oriented spins, or equivalently, to perform a total transfer of population between two energy levels.[21] This works as well on optical transitions.[22] Adiabatic passage is generally performed by sweeping the rf field frequency, while the static field remains constant. The spin is driven by an effective magnetic field $\mathbf{B}_{\text{eff}}$ whose horizontal and vertical components are, repectively, equal to the field amplitude and proportional to the detuning. As the field frequency is swept, $\mathbf{B}_{\text{eff}}$ rotates, flipping, for instance, from downward to upward orientation if the detuning is varied from negative to positive values. The spin adiabatically follows $\mathbf{B}_{\text{eff}}$ provided the rotation speed is much smaller than the precession rate of the spin around $\mathbf{B}_{\text{eff}}$. In terms of the Rabi frequency Ω and the rf frequency chirp rate r, this condition can be expressed as

$$\Omega^2 \gg r. \tag{1}$$

Vertical flip or population transfer, the most popular ARP application, does not preserve any phase shift since the initial state is orthogonal to the final one. On the contrary, spin refocusing aims at making the final superposition state coincide with the initial one. Phase control is essential. A single ARP is not enough but a pair of ARP pulses can refocus the spins in any direction.[23–25]

The principle of spin refocusing by a pair of ARP pulses is illustrated in Fig. 1. The figure represents the evolution of the phase, that is, the angular position, of two spins in the horizontal plane. The two spins differ by their detuning with respect to the center ω_0 of the inhomogeneously broadened energy spacing distribution. They are aligned at initial time $t = 0$. Then rotating at different rates around the vertical axis, they depart from each other. One applies a first ARP pulse whose frequency is linearly swept at rate r through ω_0 at time $T/4$. The pulse gets resonant with a spin of frequency ω at time $t = T/4 + (\omega - \omega_0)/r$, when the phase equals $rt(t - T/4)$.
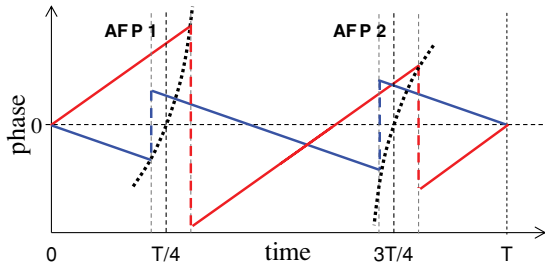
FIG. 1. (Color online) Time evolution of spin-angular positions in the horizontal plane, in a frame rotating at angular frequency ω_0. The red and blue lines correspond to two spins with different detunings with respect to ω_0. Initially aligned, the two spins return to their initial orientation at time T, after undergoing two ARP excitations centered at times $T/4$ and $3T/4$. The black dotted lines represent the locus of the flipping positions. In this representation, we neglected all relaxation processes.

At that moment the spin vertical component is flipped and the horizontal angular position is reverted. In the figure, flipping is assumed to last much less than $T/4$. Then the spin phase continues to evolve at the same rate until interaction with a second ARP pulse, identical to the first one, and centered at time $3T/4$. The interaction time is shifted by the same amount $(\omega - \omega_0)/r$ with respect to $3T/4$. This second pulse reverts the

phase again and restores the initial vertical spin component. Finally the spins are phased together again at time T. The locus of the flipping positions in the phase/time representation comprises two quadratic segments defined by $\phi = rt(t - T/4)$ and $\phi = r(T - t)(t - 3T/4)$.

A simulation of spin refocusing by a pair of successive ARP's is presented in Fig. 2. The magnetization equations of motion (see Appendix A) are numerically solved with the following parameter values: each ARP lasts for $T/2 = 0.1$ ms, during which the rf field Rabi frequency is maintained fixed at 0.28 MHz. The rf is swept at a constant rate of 0.04 MHz/μs. The 2000 spins are distributed over a 1-MHz-wide Gaussian inhomogeneous distribution. At time $t = 0$, they are all directed along axis Ox. The figure illustrates the strong scattering of spin directions at times $T/4$, $T/2$, and $3T/4$, strikingly contrasting with refocusing at time T.

III. MEASURING THE SPIN-REFOCUSING EFFICIENCY

Aiming at measuring the spin-refocusing efficiency, we have to compare the final oriented spin concentration with the initial one. This information cannot be provided by a standard spin-echo experiment. Indeed, it is difficult to relate the echo intensity to the initial spin-coherence concentration. Usually an echo experiment only gives access to the signal intensity
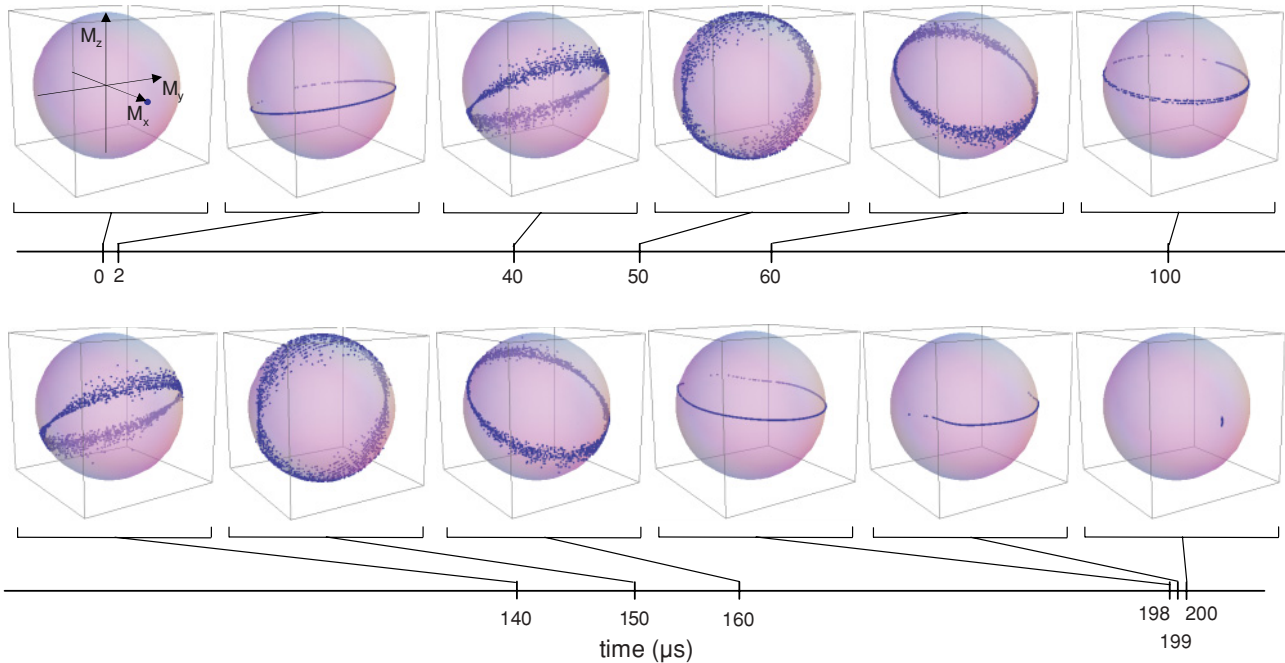
FIG. 2. (Color online) Numerical simulation of spin refocusing by a sequence of two contiguous identical ARP's. During each ARP, a fixed-amplitude rf field (Rabi frequency = 0.28 MHz) is frequency-chirped for 100 μs at the fixed rate of 0.04 MHz/μs. We consider an ensemble of 2000 spins, randomly scattered over a 1-MHz-wide Gaussian inhomogeneous distribution. The magnetization components are represented on the Bloch sphere at different stages of the rephasing, in a frame rotating at the central frequency of the inhomogeneous distribution. At time $t = 0$, all the spins are directed along Ox. The rf field scans across the 1-MHz-wide spin distribution for 25 μs and comes into resonance with the distribution center at times $t = 50$ μs and $t = 150$ μs. The displayed snapshots represent some critical stages of the spin evolution. Very rapidly, within a few microseconds corresponding to the inverse inhomogeneous width, the spins spread over a horizontal disk. As time elapses, the pancake shape is roughly preserved but the disk bounces more and more strongly as spins approach resonance with the driving field. A single ARP is not enough to refocus the spins, as can be seen at the end of the first ARP, at $t = 100$ μs. The effect of the second adiabatic passage is symmetric to the first one. Most of the spins are rephased at $t = 200$ μs. The imperfection of the refocusing is attributed to the finite value of the swept interval. Relaxation is ignored throughout the process.
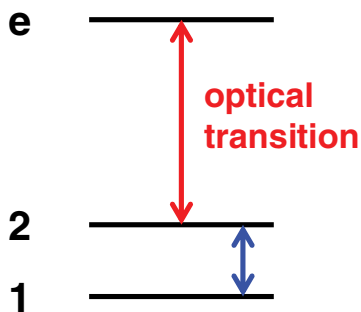
FIG. 3. (Color online) Optical probing of magnetic resonance. The upper electronic state $|e\rangle$ is optically connected to $|2\rangle$, a nuclear spin sublevel of the electronic ground state. As the $|1\rangle \rightarrow |2\rangle$ spin transition is excited by the rf field at Rabi frequency Ω, the state $|2\rangle$ population is optically probed by absorption on the $|2\rangle \rightarrow |e\rangle$ transition.

dependence on various parameters such as the pulse delay, temperature, external fields, etc. Optical absorption is a simple tool to reach the desired quantity.

Let the two states $|1\rangle$ and $|2\rangle$ of an $I = 1/2$ nuclear spin be connected by optical transitions to a common $|e\rangle$ excited state (see Fig. 3). The spins are first prepared in state $|1\rangle$ by optical pumping from state $|2\rangle$. In other words, all the spins are aligned vertically, with the same orientation. The transmitted optical intensity is originally measured as I_1 on transition $|2\rangle \rightarrow |e\rangle$. As the spins are pumped from $|2\rangle$ to $|1\rangle$, the sample absorption vanishes and the transmitted intensity raises to the input value I_0.

At time $t = 0$, one applies a rf $\pi/2$ hard pulse to rotate the overall spins into the horizontal plane. Following the pulse, the vertical spin component drops to 0, as can be monitored through the absorption increase on transition $|2\rangle \rightarrow |e\rangle$. States $|1\rangle$ and $|2\rangle$ are equally populated, which actually makes the absorption coefficient recover its original thermal equilibrium value. The transmitted intensity drops to I_1.

A $\pi/2$ hard pulse, applied immediately after the first one but with opposite sign, should be able to rotate back the spins to their original orientation. Instead, one lets the spins precess freely after the first $\pi/2$ pulse. Initially aligned, the spins begin to depart from each other in the horizontal plane, until they are evenly oriented in all directions. This occurs in a time interval equal to the inverse inhomogeneous width. After the spin direction is randomized, excitation by a $\pi/2$ hard pulse is no longer able to rotate the spins back to state $|1\rangle$ and to make the absorption vanish on transition $|2\rangle \rightarrow |e\rangle$. The transmitted intensity remains equal to I_1.

To make the absorption sensitive again to a $\pi/2$ pulse, one refocuses the spins with a pair of ARP full pulses that shine the sample at times $T/4$ and $3T/4$. At time T, the spins are aligned again. A $\pi/2$ pulse is used to rotate the spins back to vertical position. However, the horizontal spin component relaxes on a timescale $T_2 = 1/\gamma$ during the time interval T. If the spins do not totally return to state $|1\rangle$, absorption does not vanish. With exponential relaxation, at rate γ, the final absorption on transition $|2\rangle \rightarrow |e\rangle$ is reduced by factor $1 - e^{-\gamma T}$ with respect to the original value, in the medium at thermal equilibrium.

IV. REPLACING $\pi/2$ HARD PULSES BY ADIABATIC HALF-PASSAGE

Resorting to $\pi/2$ hard pulses is somehow inconsistent with previous assumptions. As already discussed, the uniform excitation of the inhomogeneously broadened spin transition would demand very hard pulses with unacceptably high power. Adiabatic passage may offer an alternative way to rotate the spin into the horizontal plane. Let us consider the transformation operated by an adiabatic half-passage (AHP) process,[24] an ARP that is interrupted at time $t = 0$, when the pulse frequency is scanned through ω_0. In order that such an interrupted ARP cannot be mistaken with a complete ARP, we denote the latter as an adiabatic full passage (AFP) in the following. We restrict the discussion to the most simple case where the rf field amplitude is kept constant over the pulse duration, although more sophisticated adiabatic schemes, such as the complex hyperbolic secant, turn out to be more popular in NMR and optical[26,27] applications.

According to Appendix A 2, the AHP turns the initially vertical spin $M(\Delta, -\infty) = (0,0,1)$ into

$$M(\Delta,0) = \frac{1}{\sqrt{\Omega^2 + \Delta^2}}(-\Omega, 0, \Delta), \qquad (2)$$

where the Rabi frequency $\Omega = \gamma_B B$ is expressed in terms of the rf field constant amplitude B and the gyromagnetic factor γ_B. The spins with large negative Δ detuning undergo an upside-down flip, while those with large positive detuning preserve their initial orientation. Hence $M_z(\Delta, 0)$ is an *odd* function of Δ. Spins with $|\Delta| < \Omega$ are rotated toward the horizontal plane, irrespective of the detuning sign.

Let the spins be distributed over a Δ_0 broad inhomogeneous width, according to an *even* distribution $G(\Delta)$, with unit normalization $\int G(\Delta)d\Delta = 1$. Then the absorption coefficient on transition $|2\rangle \rightarrow |e\rangle$ reads as

$$\alpha(t) = \alpha_0 \int G(\Delta)[1 - M_z(\Delta,t)]d\Delta. \qquad (3)$$

At equilibrium, $M_z(\Delta, -\infty) = 0$ and $\alpha(-\infty) = \alpha_0$. After pumping from $|2\rangle$ to $|1\rangle$, $\alpha(t)$ vanishes. The AHP makes $\alpha(t)$ change back to α_0 at $t = 0$, exactly as a $\pi/2$ hard pulse would do, the transmitted intensity returning to I_1.

However, the vertical spin component only vanishes on average. When AFP pulses excite the medium, the spins with different Δ values do not flip simultaneously, which is reflected by a transient variation of absorption. Let the spins evolve freely until the first AFP pulse, centered at time $T/4$, with $\Delta_0 T/4 \gg 1$. As far as absorption is concerned, inhomogeneous dephasing enables us to ignore the conversion of the horizontal components into the vertical one. Indeed this contribution vanishes when averaged over Δ. According to Appendix A 3, $M_z(\Delta, t)$ varies as

$$M_z(\Delta,t) = \frac{\Delta}{\sqrt{\Omega^2 + \Delta^2}} \frac{\Delta - \dot{\phi}(t - T/4)}{\sqrt{\Omega^2 + [\Delta - \dot{\phi}(t - T/4)]^2}}. \qquad (4)$$

The resulting variation of $\alpha(t)$, given by Eq. (3), carries information on $G(\Delta)$. After reaching a minimum,

$$\alpha(T/4) = \alpha_0 \int \frac{G(\Delta)\Omega^2}{\Omega^2 + \Delta^2} d\Delta, \qquad (5)$$

at $T/4$, $\alpha(t)$ returns to α_0, while the transmitted intensity reaches a maximum I_2 before dropping back to I_1. In a similar way, the transmitted intensity decreases during the second AFP pulse at $3T/4$.

At time T the spins are refocused as

$$M(\Delta,T) = \frac{1}{\sqrt{\Omega^2 + \Delta^2}}(-\Omega e^{-\gamma T}, 0, \Delta), \qquad (6)$$

where the transverse relaxation has been accounted for. An AHP is used again to rotate the spins back to vertical orientation. The pulse frequency is linearly swept with opposite rate with respect to the first AHP, starting at frequency ω_0 at time T. The final M_z component reads as

$$M(\Delta,+\infty) = \frac{\Omega^2 e^{-\gamma T} + \Delta^2}{\Omega^2 + \Delta^2}, \qquad (7)$$

which leads to the final absorption:

$$\alpha(T) = \alpha_0 \left(1 - e^{-\gamma T}\right) \int \frac{G(\Delta)\Omega^2}{\Omega^2 + \Delta^2} d\Delta. \qquad (8)$$

The final intensity $I_f(T)$ is related to I_0 and I_2 by

$$\ln\big(I_f(T)/I_2\big) = e^{-\gamma T} \ln(I_0/I_2). \qquad (9)$$

Should horizontal refocusing be imperfect, $e^{-\gamma T}$ should be replaced by $\eta e^{-\gamma T}$ where $\eta < 1$. Hence, the refocusing efficiency can be defined as

$$\eta = e^{\gamma T} \ln\big(I_f(T)/I_2\big) / \ln(I_0/I_2). \qquad (10)$$

Provided η does not vary with T, Eqs. (9) and (10) can be recombined into

$$\ln\big(I_f(T)/I_f(\infty)\big) = e^{-\gamma(T-T_0)} \ln\big(I_f(T_0)/I_f(\infty)\big). \qquad (11)$$

Hence, the variations of $\ln\big(I_f(T)\big)$ with T give access to the γ decay rate, irrespective of η value.

V. EXPERIMENTAL

The experiments are carried out in a 0.1 at.% Tm^{3+}:YAG crystal. An external magnetic field lifts the nuclear spin degeneracy. The resulting four-level structure is comprised of two ground states and two excited states. We choose the same field orientation as in Ref. 16.

The optical aspects of the setup have been described extensively in Refs. 16 and 18. Basically, the light beam, emerging from an external cavity diode laser, is amplitude and phase-shaped by acousto-optics modulators, driven by a high sample-rate arbitrary wave form generator (AWG). The crystal is cooled down to 1.7 K in a liquid Helium cryostat. The static magnetic field is generated by superconductive coils and is set to about 0.5 T, which leads to a ground-state splitting of 15.7 MHz. The spin transition is resonantly driven by a rf magnetic field. This excitation is supplied by a 10-turn, 20-mm-long, 10-mm-diam coil oriented along the light pulse wave vector. The crystal sits at the coil center. The rf signal, generated by the AWG, is fed to the coil through a 500-W amplifier.

First we calibrate the Rabi frequency of the spin transition, as a function of the voltage applied to the coil. To this end, we optically detect the Rabi oscillations of the spin states. Let us go back to the system described in Fig. 3. After optically pumping the ions in state $|1\rangle$, we apply the rf excitation
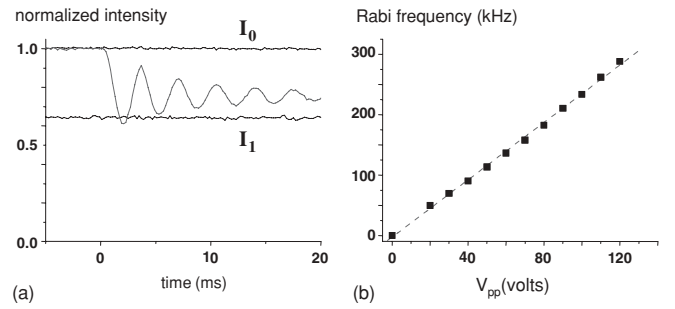
FIG. 4. Nutation experiment. (a) Time evolution of the normalized transmission through the crystal. The transmitted optical intensity, equal to I_1 when both ground state sublevels are equally populated, raises to I_0 when all spins are prepared in state $|1\rangle$. When the rf magnetic field is applied, the transmitted intensity oscillates (red line). The rf field is turned on at $t = 0$. The peak-to-peak voltage at the coil is set to 120 V. (b) Rabi frequency as a function of the applied peak-to-peak voltage.

and detect the state oscillations by monitoring the optical absorption on transition $|2\rangle \rightarrow |e\rangle$ with the help of a weak probe beam. Provided the probe intensity is low enough, the absorption coefficient is proportional to the population of $|2\rangle$ and oscillates at the Rabi frequency, as observed in Fig. 4(a). They are damped because the spins are not uniformly coupled to the rf field. This partly results from the inhomogeneous broadening of the spin transition, and from the Δ detuning dependence of the $\sqrt{\Omega^2 + \Delta^2}$ effective Rabi frequency. This also reflects the nonuniformity of the rf field over the crystal, given the finite length of the coil and the field distortions by metallic parts of the cryostat. The excitation nonuniformity also explains the limited amplitude of the oscillations in Fig. 4(a). Total inversion is not observed. From the data in Fig. 4(b), Ω is measured to vary linearly with the peak-to-peak voltage, measured at the coil input, at the rate of 2.4 ± 0.1 kHz/V.

Next we turn to the adiabatic spin refocusing experiment. We use the most simple adiabatic passage procedure where a fixed-amplitude field is frequency-chirped at constant rate r. As pointed out in Sec. II, the precession speed of the spin around the driving vector, Ω, shall be much larger than the rotation speed of the driving vector, r/Ω. In addition, the duration of the pulse shall by far exceed the time Δ_0/r needed to scan the inhomogeneous width Δ_0. Finally, since an ARP is a coherent process, the flipping time Ω/r shall be much smaller than the spin coherence lifetime. The adiabatic pulse (AFP) features are summarized in Table I.

They are expected to satisfy the three adiabatic passage conditions. The spin coherence lifetime can be deduced from the T dependence of the probe beam transmitted intensity $I_f(T)$, measured at the end of the second AHP [see Eq. (11)]. According to the experimental data, displayed in Fig. 5 [$I_f(T)/I_f(\infty)$] decays exponentially as expected,

TABLE I. Features of the adiabatic pulses used for spin refocusing.

$\Omega/(2\pi)$	$r/(2\pi)$	Duration	Ω^2/r	Ω/r
284.4 kHz	40 kHz/μs	100 μs	12.7	7.1 μs
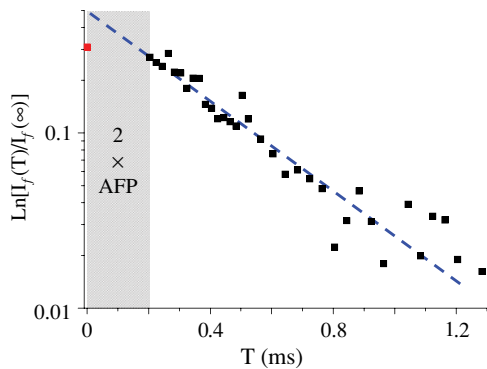
FIG. 5. (Color online) Measurement of $\ln(I_f(T)/I_f(\infty))$ as a function of delay T. Exponential decay fit leads to $\gamma^{-1} = 0.33 \pm 0.05$ ms. The dashed (red) line corresponds to exponential decay at rate $\gamma = 3.0$ ms^{-1}. The shaded area is inaccessible. Indeed, the pair of refocusing AFP's prevents us from reducing T under 200 μs. However, refocusing is not needed if one applies the second AHP just after the first one. From the measurement of $\ln(I_f(T)/I_f(\infty))$ at $T = 0$ (red dot), one infers that $I_f(T)$ decays at rate smaller than $\gamma = 3.0$ ms^{-1} from $T = 0$ to $T = 0.2$ ms.

which leads to a spin-coherence lifetime of $\gamma^{-1} = 0.33 \pm 0.05$ ms. This result is consistent with a previous Raman echo measurement.[17] The exponential decay is also consistent with photon echo experiments that were performed in a Tm^{3+}:YAG crystal at the same concentration, and in the same temperature conditions where the relaxation of both optical and spin coherences is dominated by spin-spin interaction.[28] However, the spin coherence appears to decay at a slower rate between $T = 0$ and $T = 0.2$ ms. This effect deserves further investigation.

The refocusing efficiency can now be measured. The time-evolution of the probe beam transmitted intensity is shown in Fig. 6, together with the rf adiabatic sequence.

In accordance with the storyline of Sec. IV, the incoming probe intensity I_0 is totally transmitted at the beginning, through an intially transparent material. The first AHP excitation rotates the spins into the horizontal plane, which makes the transmitted intensity drop to I_1 at time 0. Then, during the AFP refocusing steps, the transmitted intensity remains close to I_1, except around times $T/4$ and $3T/4$. It first exhibits a bump, reaching the maximum value I_2 at times $T/4$, then an antibump at time $3T/4$. Those variations correspond to the flip of the vertical spin component. Indeed only the spins at ω_0 have been perfectly rotated toward the horizontal plane by the AHP. Off-resonant spins, distributed over the $|1\rangle \rightarrow |2\rangle$ transition inhomogeneous width Δ_0, are only partially rotated and keep a vertical component. A magnified view of the bump at $T/4$ is shown in Fig. 7. We determine Δ_0 (full width at half maximum) by fitting the bump profile with Eq. (4). We obtain $\Delta_0 = 0.5 \pm 0.1$ MHz, which is consistent with previous measurements.[17]

After interaction with the two AFP's, the spins are expected to be aligned together at time T. At that moment, after changing the chirp rate sign, we use a second AHP to rotate back the spins to their initial vertical orientation. Perfect refocusing, with no decoherence, should make the transmitted intensity return to I_0. The measured transmitted intensity is denoted $I_f(T)$.
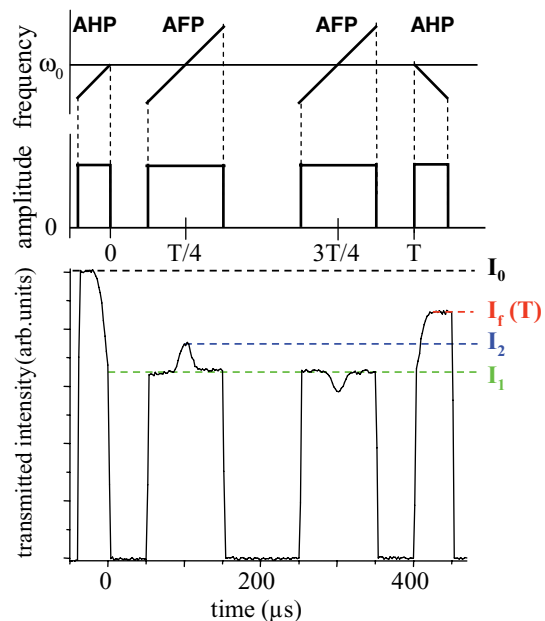
FIG. 6. (Color online) Spin-refocusing experiment in a 0.1 at.% Tm^{3+}:YAG crystal. Upper box: amplitude and frequency variations of the rf driving field. Lower box: transmitted optical intensity. The probe optical pulse is switched on only when the rf field is applied, and switched off elsewhere. After optical transfer to state $|2\rangle$ the medium is transparent (I_0). The first AHP rotates the spins and restore the equilibrium transmission (I_1). The transmitted intensity raises to a maximum I_2 during the AFP and behaves in the opposite way during the second AFP. At the end of the second AHP the transmitted intensity reaches its final $I_f(T)$ value.

Substituting the Fig. 6 experimental data and $\gamma^{-1} = 0.33$ ms into Eq. (10), we obtain $\eta = 1.6 \pm 0.3$. This unphysical value, much larger than the unit upper boundary, suggests that the spin-coherence relaxation might be slower than expected. We suspect that the 0.2 ms interval between the adiabatic passages is not much larger than the reservoir fluctuation correlation time. As a consequence, the spin decoherence might be partially suppressed by the two successive AFP's.[29,30] This is confirmed by experimental data in Fig. 5.
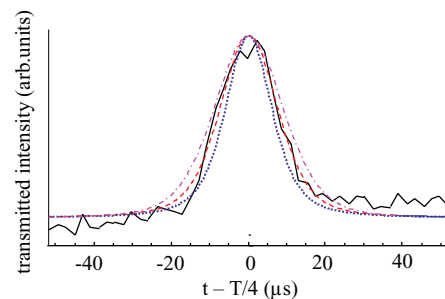
FIG. 7. (Color online) transmission bump at T/4. The transmitted optical intensity temporal profile, as derived from Eq. (4), is fitted to the experimental data, assuming a gaussian inhomogeneous distribution. The RF frequency is swept at a rate of 40 MHz/ms, and the Rabi frequency has been measured to be $\Omega/(2\pi) = 0.28$ MHz. The dotted (blue), dashed (red), and dot-dashed (magenta) lines, respectively, correspond to an inhomogeneous bandwidth (full width at half maximum) of 0.3, 0.5, and 0.7 MHz.

VI. CONCLUSION

We have used optical detection to investigate the spin-refocusing capabilities of adiabatic pulses in a Tm^{3+}:YAG crystal. As in any conventional spin-echo experiment we have measured the transverse relaxation time of the Tm^{3+} ion spin coherence in the electronic ground state. Moreover we have shown that the optical absorbance procedure gives direct access to the spin-coherence concentration. As a consequence, one can measure the spin-refocusing efficiency. Spin decoherence seems to be slowed down on time scales shorter than, or on the order of, 0.2 ms. If confirmed, this system might offer an interesting test bed for extending the Carr-Purcell Meiboom-Gill[14,31] method to adiabatic passages.

ACKNOWLEDGMENTS

APPENDIX A: ADIABATIC RAPID PASSAGE DESCRIPTION

1. ARP operator

This very standard calculation is presented for the sake of completeness. In addition, we want to point out the importance of a common reference frame in a problem where the medium undergoes successive excitations by rf fields $B_i(t)$. Those fields are swept through ω_0 at different times t_i. They can be expressed as

$$B_i(t) = B\cos[\omega_0 t + \phi(t - t_i)]. \tag{A1}$$

Instead of changing immediately to the frame rotating at the instantaneous frequency of the field, we first make a change to the common reference frame rotating at frequency ω_0. In this frame, the rotating wave approximation of the Bloch equation reads

$$\begin{cases} \partial_t M_x = -\Delta M_y - \Omega\sin[\phi(t - t_i)]\,M_z, \\ \partial_t M_y = \Delta M_x + \Omega\cos[\phi(t - t_i)]\,M_z, \\ \partial_t M_z = \Omega\sin[\phi(t - t_i)]\,M_x - \Omega\cos[\phi(t - t_i)]\,M_y, \end{cases} \tag{A2}$$

where $\Delta = \omega_{12} - \omega_0$ and the Rabi frequency $\Omega = \gamma_B B$ is expressed in terms of the rf field constant amplitude B and the gyromagnetic factor γ_B. One performs two successive changes of frame. First one transforms the spin coordinates according to the rotation $M = R_1^{(i)}M'$ where

$$R_1^{(i)}(t) = \begin{pmatrix} \cos[\phi(t - t_i)] & -\sin[\phi(t - t_i)] & 0 \\ \sin[\phi(t - t_i)] & \cos[\phi(t - t_i)] & 0 \\ 0 & 0 & 1 \end{pmatrix}. \tag{A3}$$

The new frame rotates in concert with the frequency swept field, and the Bloch equations are changed into

$$\begin{cases} \partial_t M_{x'} = -[\Delta - \dot\phi(t - t_i)]M_{y'}, \\ \partial_t M_{y'} = [\Delta - \dot\phi(t - t_i)]M_{x'} + \Omega M_{z'}, \\ \partial_t M_{z'} = -\Omega M_{y'}. \end{cases} \tag{A4}$$

To align the z'' axis along the driving vector, one performs a second transformation that is defined by the rotation $M' = R_2^{(i)}M''$, where

$$R_2^{(i)}(t) = \begin{pmatrix} \cos\Theta^{(i)} & 0 & -\sin\Theta^{(i)} \\ 0 & 1 & 0 \\ \sin\Theta^{(i)} & 0 & \cos\Theta^{(i)} \end{pmatrix}, \tag{A5}$$

where

$$\sin\Theta^{(i)} = \Omega/\Omega_{\text{eff}}, \quad \cos\Theta^{(i)} = [\Delta - \dot\phi(t - t_i)]/\Omega_{\text{eff}}$$

and

$$\Omega_{\text{eff}}(t) = \sqrt{\Omega^2 + [\Delta - \dot\phi(t - t_i)]^2}.$$

In this frame the Bloch equation reads

$$\begin{cases} \partial_t M_{x''} - M_{z''}\dot\Theta^{(i)} = -\Omega_{\text{eff}}M_{y''}, \\ \partial_t M_{y''} = \Omega_{\text{eff}}M_{x''}, \\ \partial_t M_{z''} + M_{x''}\dot\Theta^{(i)} = 0. \end{cases} \tag{A6}$$

Assuming adiabatic conditions are satisfied, one can neglect $M_{z''}\dot\Theta^{(i)}$ and $M_{x''}\dot\Theta^{(i)}$, which leads to

$$\begin{cases} \partial_t M_{x''} = -\Omega_{\text{eff}}M_{y''}, \\ \partial_t M_{y''} = \Omega_{\text{eff}}M_{x''}, \\ \partial_t M_{z''} = 0. \end{cases} \tag{A7}$$

The solution of this equation can be expressed as the following propagator:

$$U^{(i)}(t \leftarrow t') = \begin{pmatrix} \cos\Phi^{(i)} & -\sin\Phi^{(i)} & 0 \\ \sin\Phi^{(i)} & \cos\Phi^{(i)} & 0 \\ 0 & 0 & 1 \end{pmatrix}, \tag{A8}$$

where $\Phi^{(i)} = \int_{t'}^{t}\Omega_{\text{eff}}(t'')dt''$. Finally, in the common frame rotating at ω_0, the effect of an ARP on the spin coordinates can be described by the propagator

$$\begin{aligned} V^{(i)}&(t \leftarrow t') \\ &= R_1^{(i)}(t)R_2^{(i)}(t)U^{(i)}(t \leftarrow t')\left[R_1^{(i)}(t')R_2^{(i)}(t')\right]^{-1}. \end{aligned} \tag{A9}$$

2. AHP effect

The effect of the first AHP is described by $V^{(0)}(t_0 \leftarrow -\infty)$. One easily verifies that $R_2^{(0)}(-\infty) = \mathbb{1}$. As a consequence, the operator

$$U^{(0)}(t_0 \leftarrow -\infty)\left[R_1^{(0)}(-\infty)R_2^{(0)}(-\infty)\right]^{-1}$$

has no effect on the initially vertical spin $M(\Delta, -\infty) = (0,0,1)$. One can also check that $R_1^{(0)}(t_0) = \mathbb{1}$. Hence

$$M(\Delta, t_0) = R_2^{(0)}(t_0)M(\Delta, -\infty), \tag{A10}$$

where, according to Eq. (A5),

$$R_2^{(0)}(t_0) = \frac{1}{\Omega_{\text{eff}}}\begin{pmatrix} \Delta & 0 & -\Omega \\ 0 & \Omega_{\text{eff}} & 0 \\ \Omega & 0 & \Delta \end{pmatrix} \tag{A11}$$

and $\Omega_{\text{eff}} = \sqrt{\Omega^2 + \Delta^2}$. The action of the second AHP can be analyzed in a similar way.

3. AFP effect on the vertical spin component

We consider the vertical spin component evolution in the vicinity of time t_1, when the first AFP frequency comes into coincidence with ω_0. Since the spins have precessed for a time much longer than the inverse inhomogeneous width, their Δ-averaged horizontal component vanishes. Therefore, the vertical component evolves alone and, quite in the same way as in Appendix A 2, the AFP effect is completely described by $R_2^{(1)}(t)$. More specifically,

$$M_z(\Delta, t) = M_z(\Delta, t_0) \frac{\Delta - \dot{\phi}(t - t_1)}{\sqrt{\Omega^2 + [\Delta - \dot{\phi}(t - t_1)]^2}}, \quad \text{(A12)}$$

where $M_z(\Delta, t_0)$ is given by Eq. (A10).

APPENDIX B: SPIN REFOCUSING

The rf fields $B_1(t)$ and $B_3(t)$, defined according to Eq. (A1), are centered at times $t_1 = t_0 + T/4$ and $t_3 = t_0 + 3T/4$. Interacting with those fields, a spin precessing in a static field undergoes two successive identical ARP's. The

Δ detuning is $\ll \omega_0$. According to Eq. (A9), propagation from t_0 to $t_0 + T$ can be expressed as $V^{(3)}(t_4 \leftarrow t_2)V^{(1)}(t_2 \leftarrow t_0)$, where $t_2 = t_0 + T/2$. Since the two ARP's are identical, $U^{(3)}(t_4 \leftarrow t_2) = U^{(1)}(t_2 \leftarrow t_0)$, $R_j^{(1)}(t_0) = R_j^{(3)}(t_2)$, and $R_j^{(1)}(t_2) = R_j^{(3)}(t_4)$, according to the above definitions [see Eqs. (A3) and (A8)]. With the additional assumption $\phi(t) = \phi(-t)$, all the relevant $R_1^{(i)}(t_k)$ matrices are identical. It is also assumed that $\Omega \ll |\Delta| + |\dot{\phi}(t_0 - t_1)|$ so that each ARP can be completed. Then $R_2^{(1)}(t_0) \cong 1$ and

$$R_2^{(1)}(t_2) \cong \begin{pmatrix} -1 & 0 & 0 \\ 0 & 1 & 0 \\ 0 & 0 & -1 \end{pmatrix},$$

provided $\dot{\phi}(t_0 - t_1) < 0$. If $\dot{\phi}(t_0 - t_1) > 0$, the $R_2^{(1)}(t_0)$ and $R_2^{(1)}(t_2)$ expressions should be swapped. Combining all these properties, one easily shows that

$$V^{(3)}(t_4 \leftarrow t_2)V^{(1)}(t_2 \leftarrow t_0) \cong \mathbb{1}.$$

At $t_0 + T$, the three spin components return to their t_0 initial values.

*jean-louis.legouet@lac.u-psud.fr

[1] A. Kastler, J. Phys. Radium **11**, 255 (1950).

[2] A. Kastler, Physica (Utrecht) **17**, 191 (1951).

[3] J. Brossel and F. Bitter, Phys. Rev. **86**, 308 (1952).

[4] S. Geschwind, R. J. Collins, and A. L. Schawlow, Phys. Rev. Lett. **3**, 545 (1959).

[5] J. Mlynek, N. C. Wong, R. G. DeVoe, E. S. Kintzer, and R. G. Brewer, Phys. Rev. Lett. **50**, 993 (1983).

[6] W. G. Breiland, C. B. Harris, and A. Pines, Phys. Rev. Lett. **30**, 158 (1973).

[7] R. M. Shelby, C. S. Yannoni, and R. M. Macfarlane, Phys. Rev. Lett. **41**, 1739 (1978).

[8] M. Fleischhauer and M. D. Lukin, Phys. Rev. Lett. **84**, 5094 (2000).

[9] S. A. Moiseev and S. Kröll, Phys. Rev. Lett. **87**, 173601 (2001).

[10] M. Nilsson and S. Kröll, Opt. Commun. **247**, 393 (2005).

[11] R. Lauro, T. Chanelière, and J.-L. Le Gouët, Phys. Rev. A **79**, 053801 (2009).

[12] M. Afzelius, C. Simon, H. de Riedmatten, and N. Gisin, Phys. Rev. A **79**, 052329 (2009).

[13] A. V. Turukhin, V. S. Sudarshanam, M. S. Shahriar, J. A. Musser, B. S. Ham, and P. R. Hemmer, Phys. Rev. Lett. **88**, 023602 (2001).

[14] J. J. Longdell, E. Fraval, M. J. Sellars, and N. B. Manson, Phys. Rev. Lett. **95**, 063601 (2005).

[15] F. de Seze, A. Louchet, V. Crozatier, I. Lorgeré, F. Bretenaker, J.-L. Le Gouët, O. Guillot-Noël, and P. Goldner, Phys. Rev. B **73**, 085112 (2006).

[16] A. Louchet, J. S. Habib, V. Crozatier, I. Lorgeré, F. Goldfarb, F. Bretenaker, J.-L. L. Gouët, O. Guillot-Noël, and P. Goldner, Phys. Rev. B **75**, 035131 (2007).

[17] A. Louchet, Y. Le Du, F. Bretenaker, T. Chanelière, F. Goldfarb, I. Lorgeré, J.-L. Le Gouët, O. Guillot-Noël, and P. Goldner, Phys. Rev. B **77**, 195110 (2008).

[18] R. Lauro, T. Chanelière, and J. L. L. Gouët, Phys. Rev. A **79**, 063844 (2009).

[19] T. Chanelière, J. Ruggiero, M. Bonarota, M. Afzelius, and J.-L. Le Gouët, New J. Phys. **12**, 023025 (2010).

[20] M. Bonarota, J. Ruggiero, J.-L. Le Gouët, and T. Chanelière, Phys. Rev. A **81**, 033803 (2010).

[21] A. Abragam, *Principles of Nuclear Magnetism* (Oxford University Press, Oxford, United Kingdom, 1961).

[22] M. M. T. Loy, Phys. Rev. Lett. **32**, 814 (1974).

[23] S. Conolly, G. Glover, D. Nishimura, and A. Macovski, Magn. Reson. Med. **18**, 28 (1991).

[24] R. De Graaf and K. Nicolay, Concepts Magn. Reson. **9**, 247 (1997).

[25] M. Garwood and L. DelaBarre, J. Magn. Reson. **153**, 155 (2001).

[26] F. de Seze, F. Dahes, V. Crozatier, F. Bretenaker, and J. L. Le Gouët, Eur. Phys. J. D **33**, 343 (2005).

[27] L. Rippe, M. Nilsson, S. Kröll, R. Klieber, and D. Suter, Phys. Rev. A **71**, 062328 (2005).

[28] R. M. Macfarlane, Opt. Lett. **18**, 1958 (1993).

[29] B. Herzog and E. L. Hahn, Phys. Rev. **103**, 148 (1956).

[30] W. B. Mims, Phys. Rev. **168**, 370 (1968).

[31] S. Meiboom and D. Gill, Rev. Sci. Instrum. **29**, 688 (1958).